Modeling and multi-objective optimization of vacuum membrane distillation for enhancement of water productivity and thermal efficiency in desalination

Modeling and multi-objective optimization of vacuum membrane distillation for enhancement of water productivity and thermal efficiency in desalination

Dongjian Cheng [a,b], Na Li [a,b,*], Jianhua Zhang [c,*]

[a] *Department of Chemical Engineering, School of Chemical Engineering and Technology, Xi'an Jiaotong University, Xi'an, 710049, China*

[b] *Shaanxi Key Laboratory of Energy Chemical Process Intensification, Xi'an Jiaotong University, Xi'an, 710049, China*

[c] *Institute for Sustainability and Innovation, Victoria University, PO Box 14428, Melbourne, VIC 8001, Australia*

[*] Corresponding author. *E-mail address*: lina@mail.xjtu.edu.cn (N. Li)
Jianhua.Zhang@vu.edu.au (J. Zhang)

ABSTRACT

Water productivity and thermal efficiency in membrane distillation (MD) have been the main research targets, for the aims of commercial application in desalination. The comprehensive understanding of the influence of module configuration parameters, operating conditions and their interaction on MD performance is the key for MD commercialization. In this paper, the multi-objective modeling and optimization in the vacuum membrane distillation were performed by response surface methodology and desirability function approach. A series of PVDF hollow fiber modules of different scale were used to provide the essential data and to verify the modeling program. The multi-objectives including water permeate flux (J), water productivity per unit volume of module (P_v), gained output ratio (GOR), and a comprehensive index (D_m) assessing the desired MD performances were predicted and experimentally verified. The influence of operating parameters (temperature, velocity, and concentration of feed) and membrane module parameters (membrane packing density and length-diameter ratio of module) and their binary interactions on the multi-objectives was investigated. It is found that among the investigated factors, feed inlet temperature and its interaction effect with module parameters play dominant roles on MD performance. Under the multi-objective optimum conditions, 4.85×10^3 kg/(m^3•h) of P_v and 0.91 of GOR were achieved within the investigated range. Water productivity and thermal efficiency can be simultaneously enhanced by optimizing operating and module conditions with the approach developed in this study.

Keywords: Vacuum membrane distillation; Desalination; Response surface methodology; Operating conditions; Module configuration parameters

1. Introduction

Fresh water scarcity has emerged as a big challenge of the current era. Desalination of sea and brackish water has become a necessity in many arid and semiarid regions (Drioli et al., 2015). Membrane distillation (MD) is regarded to possess the potential of constituting new generation of desalination technology and has been studied actively and widely during past several decades (Drioli et al., 2015). MD is basically a thermally-driving process with only water vapor transported through porous hydrophobic membranes under a driving force of vapor pressure difference induced by a temperature difference across the membrane (Alkhudhiri et al., 2012; Drioli et al., 2015; El-Bourawi et al., 2006). The nature of driving force and hydrophobicity of membrane allows 100% theoretical rejection of non-volatile solutes. Therefore, MD is able to treat highly concentrated brine solutions to realize high water recovery under ambient pressure. Compared to commonly used desalination techniques such as multi-stage flash distillation (MSF) and multi-effect distillation (MED), MD has advantages in general lower operating temperatures (30-70°C), which permits the utilization of the low-grade or waste heat streams and the alternative energy sources (solar, wind, or geothermal) (Lawson and Lloyd, 1997).

MD integrates complex mass and heat transfer in the thermally-driving process (El-Bourawi et al., 2006). The permeate flux can be improved by increasing membrane pore size and porosity and reducing membrane thickness and pore tortuosity (Eykens et al., 2016). PVDF membrane is the most popular material used in the MD application, due to its good hydrophobicity, low thermal conductivity, and high porosity. However, the PVDF membrane fabrication process involves some toxic chemical solvents such as dimethylformamide (DMF) and 4-(dimethyl amino)pyridine (DMAP) (Samantaray et al, 2018). Chang et al. found a fabrication process using a non-toxic solvent, triethyl phosphate to prepare the PVDF hollow fiber membranes and achieved considerable MD performance (Chang et al., 2017). With the same membrane property, MD performance is strongly dependent on operating conditions and module configuration parameters (El-Bourawi et al., 2006; Wang and Chung, 2015). Operating conditions determine the driving force and affect the heat transfer coefficient in the MD process. Module configuration parameters influence the temperature and concentration polarization of stream along membrane. The comprehensive understanding of the influence of operating conditions, module configuration parameters, and their interaction on MD performance is the key for the MD commercialization.

Mathematical modeling and optimization of MD have been widely studied in optimization of membrane properties, operation conditions, and module configuration to achieve high flux and lower cost. All those studies provided references for large scale module design and process optimization (Hitsov et al., 2015; Khayet, 2011). The widely used optimization models in MD process are based on the semi-empirical Nusselt and Sherwood equations for the heat and mass transfer in the module channels and for membranes. Numerous models have been studied to predict temperature, concentration, and their polarization at the membrane surface. These equations are generally designed for a certain geometry and flow rate regime and the models cannot be reliably used for geometry optimizations (Hitsov et al., 2015). Furthermore, the membrane properties need to be characterized carefully in the modeling, which requires professional analytical instrument and long analytical procedure.

Computational fluid dynamics (CFD) method is a useful tool in both operational optimization and module design to predict the local temperature and concentration polarization, and flux and pressure drop in modules. Since the lack of proper module design has become an obstruction of significant industrial applications of MD technology, some recent CFD studies had focused on the task of module design and illustrated the effect of module dimension on total water flux and thermal efficiency of MD (Shirazi et al., 2016; Zhang et al., 2016). However, both the physical phenomenon and geometry consideration still need to be emphasized and the interaction effect of membrane fibers with high membrane packing density on MD performance has been rarely studied via CFD modeling (Hitsov et al., 2015).

In recent years, the modeling and optimization by applying response surface methodology (RSM) has attracted increasing interests (Bezerra et al., 2008). The RSM involves statistical design of various experimental factors through a set of experimental runs, and does not require complicate membrane and stream characterization, such as membrane pore size measurement, porosity measurement, membrane thickness measurement, membrane thermal conductivity measurement, etc. Therefore, the RSM provides a simple approach for the MD system performance assessment.

RSM is useful in revealing the contribution and complex interaction effect of factors with aid of visually three-dimensional plot of response. RSM has been applied successfully in various MD processes to visualize the operational space, help to understand the system behavior, and build the

mechanism knowledge base (Boubakri et al., 2014; Chang et al., 2009; Cheng et al., 2016; Cojocaru and Khayet, 2011; He et al., 2014; Khayet et al., 2012, 2007). Khayet et al. have applied RSM model to optimize water flux of direct contact membrane distillation (DCMD) process (Khayet et al., 2007) and sweeping gas membrane distillation (SGMD) process (Khayet et al., 2012) with flat sheet membrane modules. Chang et al. (Chang et al., 2009) established RS-models for multivariable optimization of separation efficiencies (defined as the ratio of produced water to the feed) of DCMD and air gap membrane distillation (AGMD) process. C. Cojocaru and M. Khayet (Cojocaru and Khayet, 2011) developed RS-models to predict permeate flux and sucrose concentration rate in SGMD with flat sheet membrane module. Boubakri et al. (Boubakri et al., 2014) used RSM to study the effects of operational parameters and initial ionic strength on DCMD permeate flux and detected the effect of interaction between feed flow rate and initial ionic strength on permeate flux. He et al. (He et al., 2014) observed the significantly positive effect of hot feed inlet temperature on both distillate flux and gained output ratio for AGMD using RSM. In our previous works (Cheng et al., 2016), the permeate flux, water productivity, and thermal efficiency of lab-scale DCMD process were modeled and optimized using RSM method as functions of both operating and module parameters.

Among the commonly studied configurations, vacuum membrane distillation (VMD) is able to have highest vapor pressure difference and thermal evaporation efficiency (Abu-Zeid et al., 2015; Cerneaux et al., 2009; Guan et al., 2014; Li and Sirkar, 2005; Tang et al., 2012). It was reported that VMD was able to achieve the similar high rejection rates to that of DCMD but achieve much higher flux (146 L/(day•m^2)) than that of DCMD (20 L/(day•m^2)) (Cerneaux et al., 2009). The thermal efficiency of the VMD process increased from 88.1% to 91.9%, in comparison with that of DCMD process increased from 59.6% to 70.5%, when the feed temperature increased from 50 to 85°C (Fan and Peng, 2012). In VMD process optimization, Mohammadi et al. applied Taguchi method (Mohammadi and Safavi, 2009) and RSM (Mohammadi et al., 2015) and determined their optimum operating conditions for maximizing permeate flux. Shin et al. introduced a new membrane de-wetting technique by using high temperature air and determined the optimum conditions by using the RSM (Y. Shin, J. Choi, T. Lee, J. Sohn, 2016). Cao et al. (Cao et al., 2016) developed an artificial neural network (ANN) model to study the performance of VMD desalination process under different operating parameters such as the feed inlet

temperature, the vacuum pressure, the feed flow rate, and the feed salt concentration. However, as far as authors' knowledge, the RSM method has not been used in modeling and optimization of VMD process using both operating conditions and module parameters as variables.

In this study, a quadratic rotation-orthogonal composite design (QRCD) and RSM has been used in modeling and optimizing VMD process with hollow fiber membrane modules for desalination of 1-9 wt% NaCl aqueous solution. For scaling up of VMD process, membrane modules with different dimension parameters and with effective membrane area ranging from 128 to 3436 cm^2 were employed. Four objectives were studied and optimized, including water permeate flux through membrane (J), water productivity per unit volume of module (P_v), gained output ratio of system (GOR), and a comprehensive index (D_m). The D_m was introduced as a comprehensive index for assessment of interaction of the other three objectives. Desirability function approach is employed to solve a multiple response optimization problem (Cojocaru et al., 2009). The variables involved in the modeling were feed inlet temperature, feed concentration, feed velocity, module packing density, and the ratio of membrane fiber length to inner diameter of the module shell (called as length-diameter ratio of module in the following). The regression models for all the objectives were established and statistically validated by variance analysis. The predicted results obtained from the models were presented in representative three-dimensional (3D) response surface plots to identify the contributions of the variables and their binary interactions on the responses. The optimum variables were determined by the desirability function approach and were verified experimentally.

2. Materials and methods

2.1. Materials and VMD apparatus

The PVDF hollow fiber membrane modules with different length-diameter ratio of module and module packing density used in this study were supplied by Tianjin Polytechnic University, China, as shown in Fig. 1. The PVDF hollow fiber membrane has average thickness of 150 μm, pore size of 0.16 μm, inner diameter of 800 μm, porosity of 85%, and liquid entry pressure of water of above 200 kPa. PVDF hollow fibers were packed into a cylindrical Plexiglas tube with outer diameter of 50 mm and inner diameter of 42 mm. The parameters of modules in the QRCD experiment including length-diameter ratio of module, module packing density, and effective membrane area, etc. were listed in Table 1.

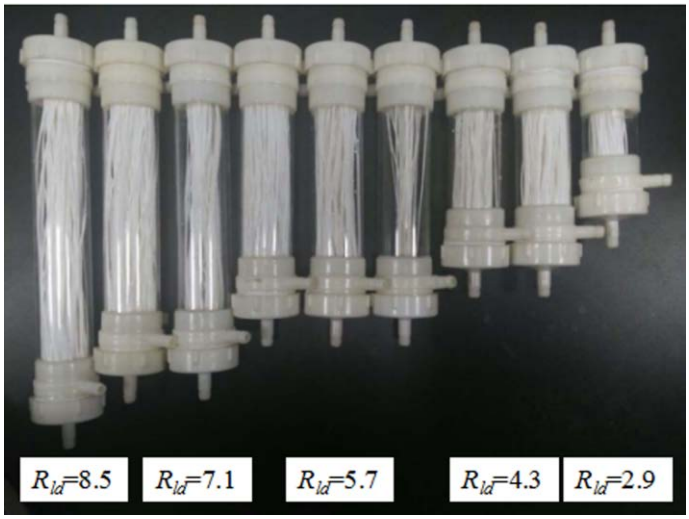

Fig. 1. Experimentally used PVDF hollow fiber membrane modules with various length-diameter ratios and packing density.

Table 1. Parameters of PVDF hollow fiber membrane modules used in the QRCD experiment.

Membrane fiber length (L), cm	Length-diameter ratio of module (R_{ld})	n[a]	Module packing density (D), %	Membrane area (A), cm^2
10	2.9	253	25	636
15	4.3	152	15	573
15	4.3	355	35	1338
20	5.7	51	5	256
20	5.7	253	25	1271
20	5.7	456	45	2291
25	7.1	152	15	955
25	7.1	355	35	2229
30	8.5	253	25	1907

[a] Number of membrane fibers in the module.

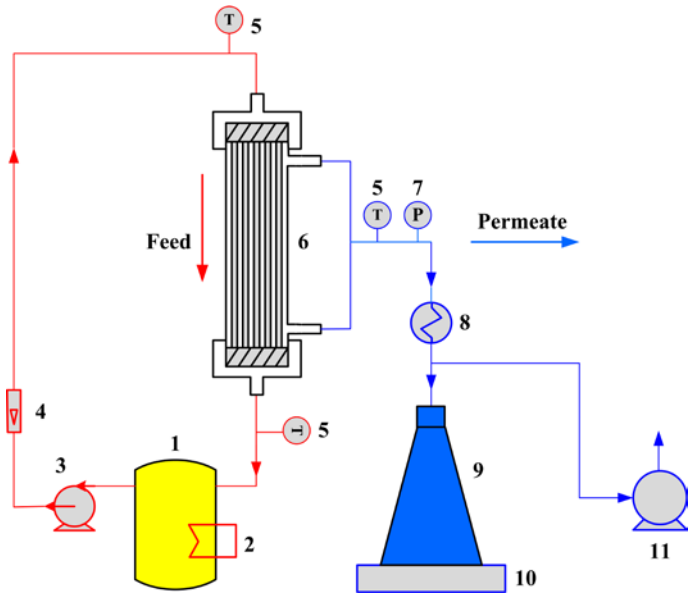

Fig. 2. Schematic diagram of VMD setup: (1) feed tank; (2) heater; (3) peristaltic pumps; (4) rotameters; (5) thermocouples; (6) hollow fiber membrane module; (7) vacuum gauge; (8) condenser; (9) permeate tank; (10) analytical balance; (11) vacuum pump.

Fig. 2 is the schematic diagram of VMD experimental set-up. The hot NaCl aqueous solution with different concentrations used as feed was circulated in the lumen side of hollow fiber membrane by a peristaltic pump and heated to a set temperature by a heater. The shell side of the module was subjected to a negative pressure by a vacuum pump. The absolute pressure on the permeate side was maintained at 2 kPa measured by a digital vacuum gauge. The feed temperatures at the inlet and outlet of the membrane module were measured by digital thermocouples with ± 0.1°C accuracy. The water vapor was condensed in a heat exchanger using 10°C chilled water. All of containers and pipes were insulted to prevent heat loss of the system. In all of the experiments, the feed volume and concentration were controlled within ± 5% variation by adding fresh water to the feed tank. The permeate weight was measured by a digital balance. The salt rejection was determined based on conductivity measurement of feed and permeate with a conductivity meter. The data were recorded when PVDF hollow fiber membrane performance was stable. The water flux was an average value for 30 min running. The relative standard deviation of water flux during each experimental run was within 4.7%. NaCl rejection was above 99.9% for all of the experimental runs.

2.2. Experimental design of VMD process

A quadratic rotation-orthogonal composite design (QRCD) and RSM were employed for

modeling and optimization of VMD. The design variables include feed inlet temperature ($T_{wf,in}$, °C), feed concentration (C_f, wt%), feed velocity (V_f, m/min), module packing density (D), and length-diameter ratio of module (R_{ld}). V_f is the linear flow velocity of feed solution in the lumen side of hollow fiber membrane. D is the ratio of the total outer cross section area of membrane to the inner cross-section area of the module. R_{ld} refers to the ratio of effective length of membrane fiber to inner diameter of membrane module shell. The variables were coded and their levels are shown in Table 2. The variable levels are adopted to be mainly in common range studied in literature. Since VMD process is feasible to treat with high concentration of solution, up to 9 wt% of high NaCl concentration was considered in the optimization.

Table 2. Coded levels and actual values of independent variables in the VMD experimental design.

Variable	Separation distance	Actual value of coded levels (α=2)				
		-α	-1	0	1	+α
Feed inlet temperature ($T_{wf,in}$), °C	10	30	40	50	60	70
NaCl concentration in feed solution (C_f), wt%	2	1	3	5	7	9
Feed velocity (V_f), m/min	4	1	5	9	13	17
Module packing density (D), %	10	5	15	25	35	45
Length-diameter ratio of module (R_{ld})	1.4	2.9	4.3	5.7	7.1	8.5

2.3. Objectives of VMD modeling and optimization

(1) Permeate flux (J, kg/(m^2•h))

J is calculated by Equation (1):

$$J = \frac{\Delta W}{At} \tag{1}$$

Here, ΔW (kg) denotes the mass variation of distillate over a given time t (h), and A (m^2) is the effective cross section area of membrane in the lumen side of the module.

(2) Water productivity per unit volume of module (P_v, kg/(m^3•h))

P_v refers to water production through per unit volume of membrane module chamber per unit operating time, which could be used to evaluate the water production capacity of a membrane module. It is calculated as follows:

$$P_v = \frac{4\Delta W}{\pi d_i^{\,2} l t} \tag{2}$$

Here, d_i (m) is the inner diameter of membrane module, l (m) is the effective length of membrane module.

P_v value reflects the overall water yielding capacity of a module. High value of P_v means high water productivity at low equipment cost and small occupied space, which is essential for economic feasibility of MD application.

(3) Gained output ratio (*GOR*)

The overall heat balance of MD system from feed side to permeate side can be expressed as below:

$$m_f H_{f,\,in} - \left(m_f - m_d\right) H_{f,\,out} = m_d \overline{H_v} + H_{Loss} \tag{3}$$

$$H_f = C_{p,f} T_{wf} \tag{4}$$

$$\overline{H_v} = H_d + \Delta H_v \tag{5}$$

Here, $H_{f,in}$ and $H_{f,out}$ are the feed stream's enthalpy (J/kg) at the inlet and outlet of a module, respectively. $\overline{H_v}$ is the average enthalpy (J/kg) of the vapor molecules. $C_{p,f}$ is specific heat of feed (J/(kg•°C)), m_f is feed flow rate (kg/h), $T_{wf,in}$ and $T_{wf,out}$ are feed temperatures (°C) at the inlet and outlet of a module, m_d is rate of permeate production (kg/h), H_d is the enthalpy (J/kg) of the permeate solution, H_{Loss} is heat loss across membrane, and ΔH_v is latent heat of evaporation (J/kg).

Then equation (3) can be rewritten as:

$$C_{p,f} m_f \left(T_{wf,in} - T_{wf,out}\right) = m_d \Delta H_f + m_d \Delta H_v + H_{Loss} \tag{6}$$

The thermal efficiency of VMD process was measured by *GOR* which is the ratio of latent heat of evaporation per unit mass of product water to total heat amount provided to feed solution from an external energy source (Summers et al., 2012; Swaminathan et al., 2016; Zhang et al., 2015):

$$GOR = \frac{m_d \Delta H_v}{C_{p,f} m_f \left(T_{wf,in} - T_{wf,out}\right)} = \frac{m_d \Delta H_v}{m_d \Delta H_v + m_d \Delta H_f + H_{Loss}} = \frac{1}{1 + \frac{\Delta H_f}{\Delta H_v} + \frac{H_{Loss}}{m_d \Delta H_v}} \tag{7}$$

GOR represents the fraction of energy used to produce fresh water product. A higher value of *GOR* corresponds to lower thermal energy consumption per unit mass of permeate.

(4) Comprehensive index (D_m)

All of the three responses (J, P_v, and *GOR*) are of practical importance, however, they are in conflict with each other as usual. For example, high module packing density is beneficial for obtaining a high value of water production capacity of membrane module (P_v), but might reduce water flux of membrane (J) and decrease energy efficiency (*GOR*). In this case, it is important to search for an optimal point to meet the requirement of users according to specific situations, such as availability of energy resources, water quantity, and limitation of operation conditions. Herein, a comprehensive evaluation index D_m is introduced for the multi-objective optimization of MD process by taking J, P_v, and *GOR* into account simultaneously via desirability function approach. Desirability function approach is a useful method to solve a multiple response optimization problem. In this method, each objective variable is converted to a normalized value in a range of 0-1. There are three forms of the desirability function depending on response's characteristics (Costa et al., 2011; Pasandideh and Niaki, 2006): (a) the-larger-the-best (LTB-type), for an objective function to be maximized; (b) the-smaller-the-best (STB-type), for an objective to be minimized; and (c) the-nominal-the-best (NTB-type), for an objective function required to achieve a particular target.

In LTB-type case, all responses could be maximized relatively. The following LTB-type equation is used to normalize the objectives:

$$d_i = \left(\frac{z_i - z_{i,min}}{z_{i,max} - z_{i,min}} \right)^{g_i}, \; i = J, P_v, GOR. \tag{8}$$

The comprehensive evaluation index D_m is calculated as a geometric mean product using the following equation:

$$D_m = \left(d_1 \bullet d_2 ... d_i ... d_m \right)^{1/m} = \left(\prod_{i=1}^{m} d_i \right)^{1/m} \tag{9}$$

Here, d_i denotes the normalized objective variable i; z_i, $z_{i,min}$, and $z_{i,max}$ are the actual, minimum, and maximum values of the optimization objective i, respectively; g_i is the weight coefficient in a range of 0-1; m is the number of responses.

It should be noted that the larger the weight coefficient value g_i in equation (8), the greater

the dominance of the corresponding single objective is. As an example, for the optimization of MD process applied in arid coastal areas when the low-grade heat source like solar energy, geothermal energy or waste heat from industry is sufficient and can be effectively used in MD process, high water production (P_v) may be of key importance and thus g_{Pv} could be higher than g_{GOR} and g_J. On the other hand, if the footprint and energy consumption account for the main cost during the operating process, g_{GOR} should be high. In case of equal importance of the three single objectives, the values of g_J, g_{Pv}, and g_{GOR} could be the same.

Actually, many different combinations of weight coefficient can be chosen. In general, the weight coefficients can be determined by means of Delphi method (expert consultation method), order relation analysis method (G1-method), and statistical method (Qian et al., 2014; Tricco et al., 2016). In this study, the statistical method was employed to determine the weight coefficients based on the minimization of average relation error (*ARE*) and Marquradt's percent standard deviation (*MPSD*) between the experimental and predicted values of D_m. For practical use, weight coefficients can be further adjusted considering process cost and users' requirement to have a desired MD performance. *ARE* and *MPSD* were calculated according to following equations (Cheng et al., 2016):

$$ARE=\frac{100}{n}\sum_{i=1}^{n}\left(\frac{\left|Y_{exp}-Y_{calc}\right|}{Y_{exp}}\right)_i \tag{10}$$

$$MPSD=100\left[\sqrt{\frac{1}{n-d}\sum_{i=1}^{n}\left(\frac{Y_{exp}-Y_{calc}}{Y_{exp}}\right)^2_i}\right] \tag{11}$$

Here, Y_{exp} refers to the experimental objective value, Y_{calc} denotes the calculated objective value by multiple regression model, n is the number of data points and d is the number of the regression coefficient.

3. Results and discussion

3.1. Determination and verification of modeling program

According to QRCD, a total number of 36 experiments (1/2 design, M_c=16, M_r=10, M_0=10) were carried out. The QRCD experimental matrix and responses are given in Table 3. The experimental design and data analysis were performed with statistical and graphical analysis

1 software - Statistical Product and Service Solutions.

2 **Table 3.** Quadratic rotation-orthogonal composite design and experimental results for VMD.

Run	$T_{wf,in}$, ℃	C_f, wt%	V_f, m/min	D, %	R_{ld}	J, kg/(m^2•h)	P_v, kg/(m^3•h)	GOR	D_m[a]
1	40	7	5	15	4.3	1.49	410.2	0.76	0.497
2	60	3	5	15	4.3	7.19	1981.6	0.95	0.901
3	40	3	13	15	4.3	1.57	433.3	0.89	0.576
4	60	7	13	15	4.3	6.29	1733.2	0.86	0.818
5	40	3	5	35	4.3	1.03	664.4	0.91	0.581
6	60	7	5	35	4.3	2.84	1831.4	0.86	0.747
7	40	7	13	35	4.3	1.02	655.7	0.70	0.413
8	60	3	13	35	4.3	4.99	3212.2	0.90	0.874
9	40	3	5	15	7.1	0.95	263.4	0.95	0.524
10	60	7	5	15	7.1	3.21	883.9	0.89	0.703
11	40	7	13	15	7.1	1.17	324.1	0.76	0.461
12	60	3	13	15	7.1	6.21	1710.6	0.94	0.863
13	40	7	5	35	7.1	0.55	382.4	0.93	0.472
14	60	3	5	35	7.1	1.91	1333.8	0.92	0.701
15	40	3	13	35	7.1	0.74	521.8	0.86	0.516
16	60	7	13	35	7.1	1.92	1347.0	0.77	0.629
17	30	5	9	25	5.7	0.34	153.8	0.68	0
18	70	5	9	25	5.7	4.44	2036.5	0.89	0.809
19	50	5	1	25	5.7	1.36	623.9	0.97	0.657
20	50	5	17	25	5.7	2.26	1037.7	0.83	0.658
21	50	5	9	5	5.7	5.46	504.8	0.87	0.683
22	50	5	9	45	5.7	1.13	931.6	0.80	0.572
23	50	5	9	25	2.9	3.38	1551.2	0.82	0.724
24	50	5	9	25	8.5	1.37	626.8	0.79	0.556
25	50	1	9	25	5.7	2.95	1356.2	0.92	0.745

26	50	9	9	25	5.7	1.58	725.8	0.75	0.544
27	50	5	9	25	5.7	1.91	875.3	0.79	0.606
28	50	5	9	25	5.7	1.81	829.8	0.80	0.590
29	50	5	9	25	5.7	1.96	899.1	0.79	0.619
30	50	5	9	25	5.7	1.76	805.9	0.80	0.604
31	50	5	9	25	5.7	1.87	857.9	0.80	0.622
32	50	5	9	25	5.7	1.92	879.6	0.80	0.617
33	50	5	9	25	5.7	1.94	890.4	0.79	0.622
34	50	5	9	25	5.7	1.87	857.9	0.79	0.606
35	50	5	9	25	5.7	1.72	790.8	0.80	0.604
36	50	5	9	25	5.7	1.84	844.9	0.80	0.607

[a] D_m was calculated with 1/3, 1/3, and 1/3 weight coefficient of *J*, P_v, and *GOR*.

Regression models of *J*, P_v, *GOR*, and D_m established based on the above experiment results are shown in Table 4. The high value of the fitting coefficients indicated the statistical validity of the RS-models. The significance of the regression coefficients in the models was evaluated using the statistical Student's t-test (Cojocaru and Khayet, 2011). The P-values were used as a tool to check the significance of each of the interactions among the variables (Ravikumar et al., 2005). Only the most significant terms with $P < 0.05$ are remained in the simplified equations in Table 5. The positive or negative value of the coefficients of items in the equations indicated the positive or negative function of the variables and interaction effect of the binary variables on the corresponding objectives.

It should be noted that the specific multiple regression model of D_m was dependent on various combinations of weight coefficients of *J*, P_v, and *GOR* according to Equations (8) and (9). Tables 4 and 5 only list the D_m models corresponding to 1/3, 1/3, and 1/3 weight coefficients of *J*, P_v, and *GOR*. Table 6 presents the calculated *ARE* and *MPSD* between the experimental and predicted values of D_m with different series of weight coefficients of *J*, P_v, and *GOR*. It can be seen that *ARE* and *MPSD* were minimum when the weight coefficients of *J*, P_v, and *GOR* were all 1/3. Considering the minimum values of *ARE* and *MPSD*, the regression model of D_m based on equal value of weight coefficients of *J*, P_v, and *GOR* in Tables 4 and 5 were adopted in the

following part.

Table 4. Multiple regression models of permeate flux (J), water productivity per unit volume of module (P_v), gained output ratio (GOR), and comprehensive index (D_m) as functions of variables and their fitting coefficients.

	Multiple regression model	Fitting coefficient/R^2
J	$=0.1877T_{wf,in}+0.1229C_f-0.5049V_f-0.0766D-0.4934R_{ld}+0.026T_{wf,in}C_f+0.0115T_{wf,in}V_f-0.0086T_{wf,in}D-0.0315T_{wf,in}R_{ld}-0.0186C_fV_f+0.0125C_fD+0.0496C_fR_{ld}-0.0026V_fD+0.0164V_fR_{ld}+0.0083DR_{ld}+0.0035T_{wf,in}^2+0.0534C_f^2+0.0042V_f^2+0.0047D^2+0.0881R_{ld}^2$	0.992
P_v	$=12.4866T_{wf,in}-50.0085C_f-128.6744V_f+0.0862D-43.7541R_{ld}-4.4645T_{wf,in}C_f+1.8517T_{wf,in}V_f+1.2217T_{wf,in}D-11.4830T_{wf,in}R_{ld}-1.9972C_fV_f-4.1822C_fD+17.7492C_fR_{ld}+3.0896V_fD+2.2367V_fR_{ld}-7.0473DR_{ld}+0.8993T_{wf,in}^2+12.6849C_f^2-1.0002V_f^2-0.2566D^2+43.8117R_{ld}^2$	0.987
GOR	$=0.0233T_{wf,in}-0.0544C_f-0.0092V_f-0.006D+0.1208R_{ld}+3.1699\times10^{-5}T_{wf,in}C_f+0.0002T_{wf,in}V_f-0.0002T_{wf,in}D-0.0022T_{wf,in}R_{ld}-0.0022C_fV_f+0.0002C_fD+0.0017C_fR_{ld}-0.0005V_fD-0.0033V_fR_{ld}-0.0002DR_{ld}-5.0419\times10^{-5}T_{wf,in}^2+0.0034C_f^2+0.0018V_f^2+0.0001D^2+0.0016R_{ld}^2$	0.998
D_m	$=0.0560T_{wf,in}-0.0812C_f-0.0578V_f-0.0110D-0.1519R_{ld}-0.0002T_{wf,in}C_f+0.0007T_{wf,in}V_f-3.5415\times10^{-6}T_{wf,in}D-0.0010T_{wf,in}R_{ld}-0.0015C_fV_f-2.3117\times10^{-5}C_fD+0.0050C_fR_{ld}-0.0001V_fD+0.0021V_fR_{ld}+0.0002DR_{ld}-0.0004T_{wf,in}^2+0.0053C_f^2+0.0013V_f^2+0.0002D^2+0.0108R_{ld}^2$	0.996

Table 5. Simplified multiple regression models of permeate flux (J), water productivity per unit volume of module (P_v), gained output ratio (GOR), and comprehensive index (D_m) as functions of variables and their fitting coefficients.

	Multiple regression model	Fitting coefficient/R^2
J	$=0.0056T_{wf,in}^2-0.0086T_{wf,in}D-0.0092T_{wf,in}R_{ld}-0.0280T_{wf,in}C_f+0.0049D^2+0.0022T_{wf,in}V_f+0.0729C_f^2+0.0179C_fD$	0.982

P_v	$=0.9822T_{wf,in}^2-11.3165T_{wf,in}R_{ld}-3.1884C_fD+0.9598T_{wf,in}D+42.6046R_{ld}^2+1.0856V_fD-5.2971DR_{ld}$	0.975
GOR	$=0.0228T_{wf,in}+0.1741R_{ld}-0.0034T_{wf,in}R_{ld}-0.0382V_f+0.0017V_f^2-0.0222C_f-0.0011D$	0.997
D_m	$=0.0431T_{wf,in}-0.0003T_{wf,in}^2-0.0020C_f^2-0.1637R_{ld}-0.0030D+0.0119R_{ld}^2-0.0380V_f+0.0007T_{wf,in}V_f$	0.992

Table 6. Error results calculated according to Equations (10) and (11) with various weight coefficients of permeate flux (J), water productivity per unit volume of module (P_v), and gained output ratio (GOR) for determination of comprehensive index (D_m).

NO.	*ARE*, %	*MPSD*, %	Weight coefficient		
			g_J	g_{Pv}	g_{GOR}
1	4.1	5.2	1/3	1/3	1/3
2	6.2	9.4	3/10	3/10	2/5
3	6.4	9.3	3/5	1/5	1/5
4	10.1	13.6	3/10	2/5	3/10
5	10.3	14.2	2/5	3/10	3/10
6	12.4	16.7	1/5	3/10	1/2
7	14.7	19.3	2/5	1/5	2/5
8	15.5	20.3	1/2	1/5	3/10
9	17.9	23.1	3/10	1/5	1/2
10	23.1	33.1	1/5	2/5	2/5

The simplified multiple regression models were tested for statistical validation using analysis of variance (ANOVA). Fischer distribution (F-test) is used to determine the F-value, which is the ratio of the mean square value of model to residual (Khayet et al., 2012). P-value can be calculated from the F-value and the degree of freedoms, and when P-value is less than 0.05, the model is statistically validated for prediction of response (Cojocaru and Khayet, 2011). The values of the statistical estimators such as F-value, P-value, R^2, and adjusted R^2 are presented in Table 7. The F-values are quite high and the P-values are below 0.0001. In addition, the R^2 values of the

regression models shown in Table 5 are greater than 0.9 and close to the adjusted R_{adj}^2 values in Table 7. Obviously, the RS-models are statistically valid.

Table 7. ANOVA results of the simplified quadratic models of average permeate flux (J), water productivity per unit volume of module (P_v), gained output ratio (GOR), and comprehensive index (D_m).

Objective	Different items	DF	Sum of squares	Mean square	F-value	P-value	R^2_{adj}
	Model	8	807.695	100.962	195.739	< 0.0001	0.977
J	Residual	28	14.958	0.516			
	Total	36	822.653				
	Model	6	5.204×10^{7}	7.434×10^{6}	168.489	< 0.0001	0.969
P_v	Residual	30	1.324×10^{6}	4.412×10^{4}			
	Total	36	5.336×10^{7}				
	Model	6	2.845×10^{-7}	1.974	492.144	< 0.0001	0.989
GOR	Residual	30	0.120	0.004			
	Total	36	13.936				
	Model	8	14.597	1.825	439.412	< 0.0001	0.990
D_m	Residual	28	0.116	0.004			
	Total	36	14.714				

The significance of the regression coefficients of the variables in the models was determined by the statistical Student 't'-test. The determined dominance degrees of the variables are shown in Table 8. It can be seen that $T_{wf,in}$ is the most significant factor for all of the four responses. The interaction effect of $T_{wf,in}$ with D and R_{ld} plays important role on J, P_v, and GOR. The most important factors on J and P_v are interaction effect of operating conditions and module parameters besides $T_{wf,in}$. GOR is mainly dominated by $T_{wf,in}$, R_{ld}, and their interaction. CI depends on $T_{wf,in}$ and other single factor including both operating condition and module parameter.

Table 8. Dominance degree of the effects of variables and their interactions on average permeate flux (J), water productivity per unit volume of module (P_v), gained output ratio (GOR), and comprehensive index (D_m).

Objective	Dominance degree of the effects of variables and their interactions
J	$T_{wf,in}^2 > T_{wf,in}D > T_{wf,in}R_{ld} > T_{wf,in}C_f > D^2 > T_{wf,in}V_f > C_f^2 > C_fD$
P_v	$T_{wf,in}^2 > T_{wf,in}R_{ld} > C_fD > T_{wf,in}D > R_{ld}^2 > V_fD > DR_{ld}$

GOR	$T_{wf,in}>R_{ld}>T_{wf,in}R_{ld}>V_f>V_f^2>C_f>D$
CI	$T_{wf,in}>T_{wf,in}^2>C_f^2>R_{ld}>D>R_{ld}^2>V_f>T_{wf,in}V_f$

The predicted responses by the multiple regression models were compared with the experimental results (from Table 3) in Fig. 3. The average relative errors for J, P_v, GOR, and D_m are 7.8%, 8.9%, 3.6%, and 6.7%, respectively.

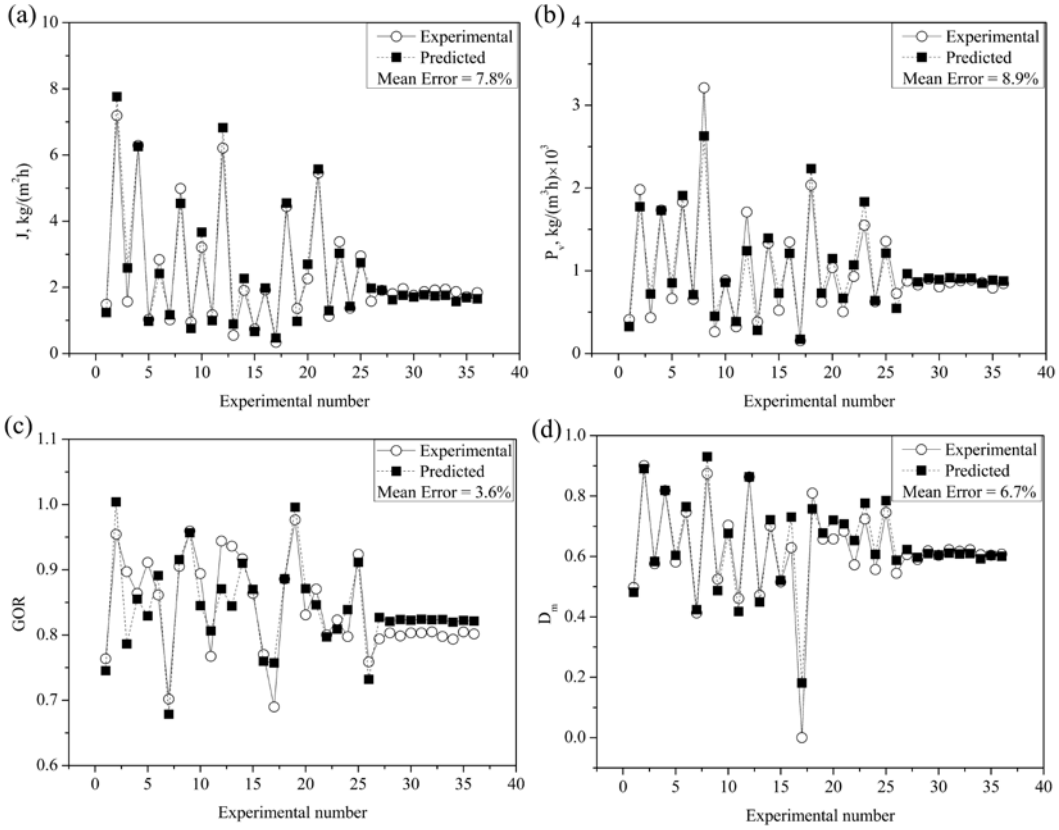

Fig. 3. Comparison between experimental and predicted VMD permeate flux (J) (a), water productivity per unit volume of module (P_v) (b), gained output ratio (GOR) (c), and comprehensive index (D_m) (d).

The empirical models were further verified experimentally as listed in Table 9. The results are shown in Fig. 4. The predicted trend for each objective agrees well with the experiment data. The average relative errors for J, P_v, GOR, and D_m are 7.1%, 8.2%, 6.2%, and 8.5%, respectively.

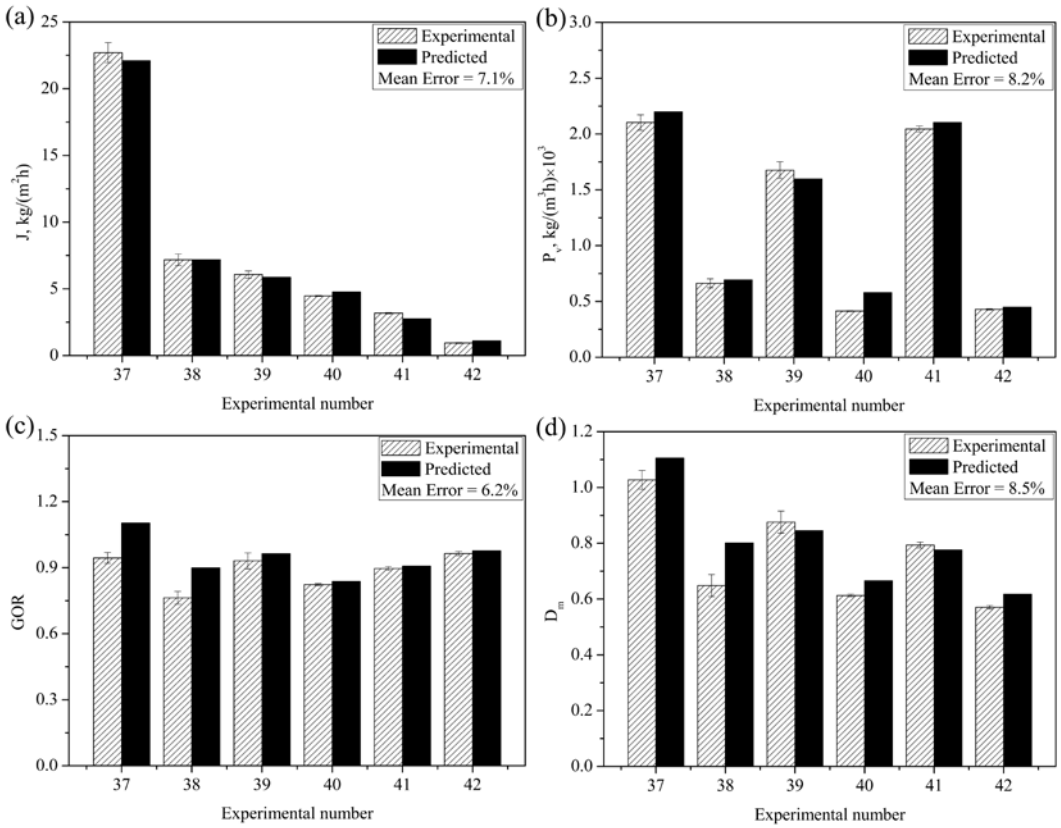

Fig. 4. Comparison between experimental and predicted VMD permeate flux (*J*) (a), water productivity per unit volume of module (P_v) (b), gained output ratio (*GOR*) (c) and comprehensive index (D_m) (d) under conditions in Table 9.

Table 9. Some experimental results performed for the validation of RSM models of VMD process.

Run	$T_{wf,in}$, °C	C_f, wt%	V_f, m/min	D, %	R_{ld}	J, kg/(m²•h)	P_v, kg/(m³•h)	GOR	D_m
37	69.1	1	17	5	4.8	22.7	2102.8	0.94	1.02
38	51.9	5	17	5	5.7	7.18	662.9	0.76	0.65
39	54	3	5	15	4.3	6.07	1675.4	0.92	0.88
40	47.4	5	9	5	5.7	4.47	413.8	0.82	0.61
41	60.7	7	5	35	4.3	3.18	2045.1	0.89	0.79
42	45.5	5	1	25	5.7	0.94	429.0	0.96	0.57

3.2. Response surface plots

The response surface curves of *J*, P_v, *GOR*, and D_m were plotted using Matlab software to investigate the interaction effect of the studied variables. Based on the statistical Student 't'-test,

only the variables with most significant influence on the objectives are illustrated in Figs. 5-9. Crossing line of the plots means there is interaction effect of two variables on response (Boubakri et al., 2014; Cheng et al., 2016).

3.2.1. Binary effect of feed inlet temperature and feed velocity

Fig. 5 (a-d) is the response surface of permeate flux (J), water productivity per unit volume of module (P_v), gained output ratio (GOR), and comprehensive index (D_m), respectively, as function of the binary effects of feed inlet temperature ($T_{wf,in}$) and feed velocity (V_f). There are interaction effects between $T_{wf,in}$ and V_f on all the objectives.

As to the effect of $T_{wf,in}$, both J and P_v increase exponentially. The permeate flux in VMD process can be expressed as follows (El-Bourawi et al., 2006; Lawson and Lloyd, 1997):

$$J = B_m\left(P_{mf} - P_{mp}\right) = B_m\left(a_{wf}P^0{}_{mf} - P_{mp}\right) = B_m\left(x_{mf}\gamma_{wf}P^0{}_{mf} - P_{mp}\right) \quad (12)$$

$$P^0{}_{mf} = exp\left(23.273 - \frac{3841.2}{T_{mf} - 45}\right) \quad (13)$$

Here, B_m is the membrane distillation coefficient, P_{mf} is the water vapor pressure on the feed side, P_{mp} is the permeate vacuum pressure, x_{mf} is the mole fraction of the solute at the membrane interface, a_{wf} and γ_{wf} are the water activity and activity coefficient, respectively, and $P^0{}_{mf}$ is pure water vapor. As illustrated in Equations (12) and (13), the exponential increase of J and P_v with $T_{wf,in}$ is due to an exponential increase of vapor pressure of feed solution with $T_{wf,in}$.

The GOR increases linearly with the increase of $T_{wf,in}$. The increase of GOR with $T_{wf,in}$ demonstrates an increased thermal efficiency in VMD. 55.9% increase of GOR is achieved by increasing $T_{wf,in}$ from 30 to 70°C at 17 m/min of V_f. Furthermore, the increase of J, P_v, and GOR with $T_{wf,in}$ would also lead to a significant increase of D_m with $T_{wf,in}$.

In Fig. 5, J and P_v increase linearly with V_f, due to the increase of driving force for mass transfer across the membrane by alleviating concentration and temperature polarization and increasing average feed temperature in the module (Bouchrit et al., 2015; El-Bourawi et al., 2006). The mitigation of concentration polarization leads to the increase of water activity (a_{wf}) as well as the vapor pressure on feed side, as presented in Equation (12). Similarly, the membrane surface temperature/the vapor pressure on feed side (Equation (13)) will increase as temperature

polarization reduces. Therefore, the driving force across the membrane can be enhanced as well. Furthermore, as the residency time of the feed in the module is reduced, the average feed temperature is also increased, which also boosts the flux. Due to the interaction effect of V_f with $T_{wf,in}$**,** the influence of one factor to another factor is more significant, when the other factor is at a higher level. For example, increasing V_f from 1 to 17 m/min at $T_{wf,in}$ of 40°C leads to 27.9% and 33.5% increase of J and P_v, respectively, and by 47.2% and 52.8% increase of J and P_v respectively at $T_{wf,in}$ of 70°C. Therefore, high $T_{wf,in}$ combined with high V_f would favor both high J and P_v.

Fig. 5 (c) shows that the *GOR* decreases initially and then goes up slightly by increasing V_f. This phenomenon can be understood based on Equation (7). As V_f increases, the thermal and concentration boundary layer on membrane surface decreases and mass and heat transfer coefficient increases. Furthermore, a higher V_f also means a shorter residence time of hot feed in the membrane module, leading to a higher average temperature on membrane surface. Consequently, feed temperature on membrane surface increases, which leads to the increase of H_f and H_{Loss} (Perry and Green, 1998). According to Equation (7), the competition between $\Delta H_f/\Delta H_v$ and $H_{Loss}/m_d\Delta H_v$ determines the trend of *GOR*. On one side, when V_f is small, increasing V_f causes the efficient increase of $\Delta H_f/\Delta H_v$ thus decreasing *GOR*. On the other side, further increasing V_f leads to a great increase of $m_d\Delta H_v$ since m_d is in an exponential relationship to the temperature on the feed side of membrane, which results in the increase of *GOR*. However, the circulation energy consumption in the MD system will increase with the increase of feed velocity, which should be taken into account when optimizing the system energy efficiency.

In Fig. 5 (d), the variation of D_m with V_f is complicated since it integrates the varying trends of J, P_v, and *GOR*. It can be seen that increasing V_f has a negative effect on D_m at low $T_{wf,in}$ while shows a positive effect at high $T_{wf,in}$. This phenomenon is due to the trade-off effect among J, P_v, and *GOR* as function of V_f. Obviously, the combination of high $T_{wf,in}$ with high V_f is the most favorite condition for a high value of D_m since it is beneficial to acquire high J, P_v, and *GOR* as shown in Fig. 5 (a-c).

In general, the synergistic effect of high feed temperature ($T_{wf,in}$) with high feed velocity (V_f) basically meets a desired performance of MD process on both high production and low energy consumption. In addition, it should be mentioned that the result is obtained at certain values of D

and R_{ld} which correspond to zero value of their coded level in Table 2. It can be anticipated that when D and R_{ld} are high, the coordination of $T_{wf,in}$ and V_f will become more vital since the concentration and temperature polarization as well as heat loss tend to become serious with the increase of D and R_{ld}.

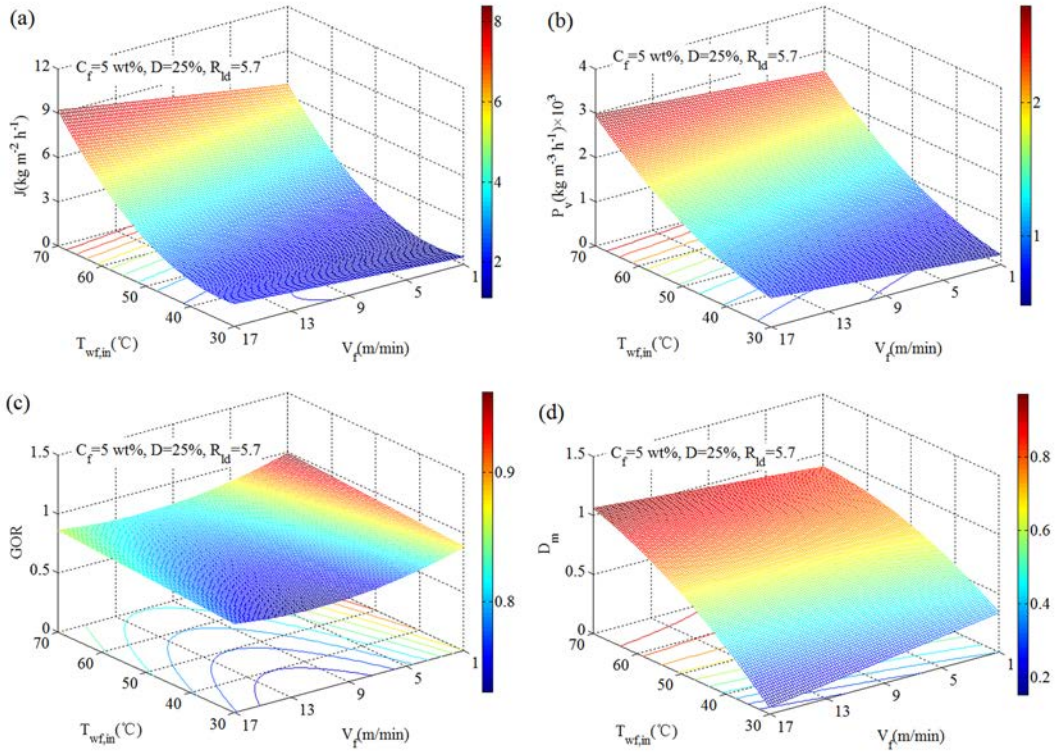

Fig. 5. Effects of feed inlet temperature ($T_{wf,in}$) and feed velocity (V_f) on (a) permeate flux (J), (b) water productivity per unit volume of module (P_v), (c) gained output ratio (GOR), and (d) comprehensive index (D_m) in 3D response surface plots.

3.2.2. Binary effect of feed inlet temperature and module packing density

The effects of feed inlet temperature ($T_{wf,in}$) and module packing density (D) on the permeate flux (J), water productivity per unit volume of module (P_v), gained output ratio (GOR), and comprehensive index (D_m) are presented in Fig. 6 (a-d). All objectives show increasing trend with increase of $T_{wf,in}$ as in Fig. 5. The interaction effect of $T_{wf,in}$ and D on J and P_v is prominent while on GOR and D_m is slight.

In Fig. 6 (a), J is almost not affected by D when $T_{wf,in}$ is as low as 30°C but with the increase of $T_{wf,in}$, J is gradually impacted by the level of D. The reason is that when $T_{wf,in}$ is low, J is also very low so that not much difference can be observed for different packing density. But for high

$T_{wf,in}$, J can be largely compromised by high D because the effective temperature is comparably lower. In the meanwhile, the increase in permeate vapor product will cause the rise of permeate temperature (T_{wp}) due to more heat transport of vapor through membrane (Lian et al., 2016). This is confirmed by the experimental data in Table 10. As can be seen, when $T_{wf,in}$, V_f, and R_{ld} keep constant, increasing D leads to the increase of feed outlet temperature ($T_{wf,out}$) and permeate temperature (T_{wp}) and the decrease of J. In addition, high D increases the probability of membrane contacting with each other, which leads to the formation of "dead zones" and thus reduces the effective membrane area for mass transfer (Lipnizki and Field, 2001; Yang et al., 2011). Additionally, when vapor condensation occurs on the permeate side of membrane, it will aggravate the contacting of membrane and further decrease effective membrane area for evaporation.

Table 10. Effect of module packing density (D) on feed outlet temperature ($T_{wf,out}$), permeate temperature (T_{wp}), and water permeate flux (J).

D, %	V_f, m/min	R_{ld}	$T_{wf,in}$, °C	$T_{wf,out}$, °C	T_{wp}, °C	J, kg/(m^2•h)
15	5	7.1	59.9	49.3	50.5	3.21
35	5	7.1	59.7	53.7	54.0	1.91
15	13	4.3	40.1	38.9	33.6	1.57
35	13	4.3	40.2	39.4	34.9	1.02

Fig. 6 (b) shows that P_v increases exponentially with the increase in $T_{wf,in}$, and increasing D leads to significant improvement of P_v at high $T_{wf,in}$. The increase of P_v with D is due to the increase of membrane area packed in the module which enlarges the evaporation area of the feed. Compared with Fig. 6 (a), it can be seen that the trend of J is reverse to P_v by increasing D at high $T_{wf,in}$. P_v is expected to be able to further increase, if J could be increased by changing other conditions such as V_f and R_{ld}. From the previous discussion, it is believed that increasing V_f is an efficient way to alleviate the negative impact from increasing D on J, which will lead to the improvement of P_v.

The effect of $T_{wf,in}$ and D on GOR is slight in Fig. 6 (c). The increase of D in the whole investigation range, i.e. from 5% to 45%, at $T_{wf,in}$ of 70°C results in only 5.4% decrease in GOR. According to Equation (7), the relatively stable GOR means the simultaneous variation of the

latent heat of evaporation ($m_d \Delta H_v$) and the total thermal consumption provided to the feed solutions ($C_{p,f} m_f (T_{wf,in} - T_{wf,out})$) as function of D. Since V_f is fixed in Fig. 6 (c), the mass flow rate (m_f in Equation (7)) increases simultaneously with the increase of D. Therefore, the amount of heat provided to the feed solutions from an external energy source increases. Meanwhile, the rate of permeate productivity also increases with the increase of D, resulting in the increase of latent heat transferred with the produced water. This consequently leads to relatively stable *GOR* with different packing density especially at high $T_{wf,in}$. A slight decrease of *GOR* is related to the variation of the thermal conductivity loss (H_{loss}) and the rate of permeate production (m_d) according to Equation (7). Feed outlet temperature ($T_{wf,out}$) increases with the increase of D as shown in Table 10. This will cause the increase of membrane surface temperature and thus lead to almost linear increase of heat conductivity loss (H_{loss}). However, the increase of m_d with increasing D is not linear since J decreases with D as shown in Fig. 6 (a). This finally results in a slight decrease of *GOR* with D.

Fig. 6 (d) indicates that $T_{wf,in}$ has a significant effect on D_m, while that of D on D_m is very slight, which is due to that J, P_v, and *GOR* are nearly not influenced by D at low $T_{wf,in}$ shown in Figs. 6 (a), (b), and (c). At high $T_{wf,in}$, an obvious trade-off effect exists between J and P_v, and *GOR* changes little as function of D, leading to a relatively stable D_m with D. Obviously, increasing $T_{wf,in}$ is a feasible way to achieve a noticeable enhancement of D_m.

From the above discussion, it can be seen that increasing D has slight effect on thermal efficiency (*GOR*) but plays significantly positive role on improving P_v. That is to say, the synergistic function of large D and high $T_{wf,in}$ could endow MD process with high level of water productivity and thermal efficiency. Although increasing D at high $T_{wf,in}$ causes a significant decrease of J which results in a slight decrease of D_m, high productivity (P_v) will be achieved at the same time, which is of more practical importance for MD application.

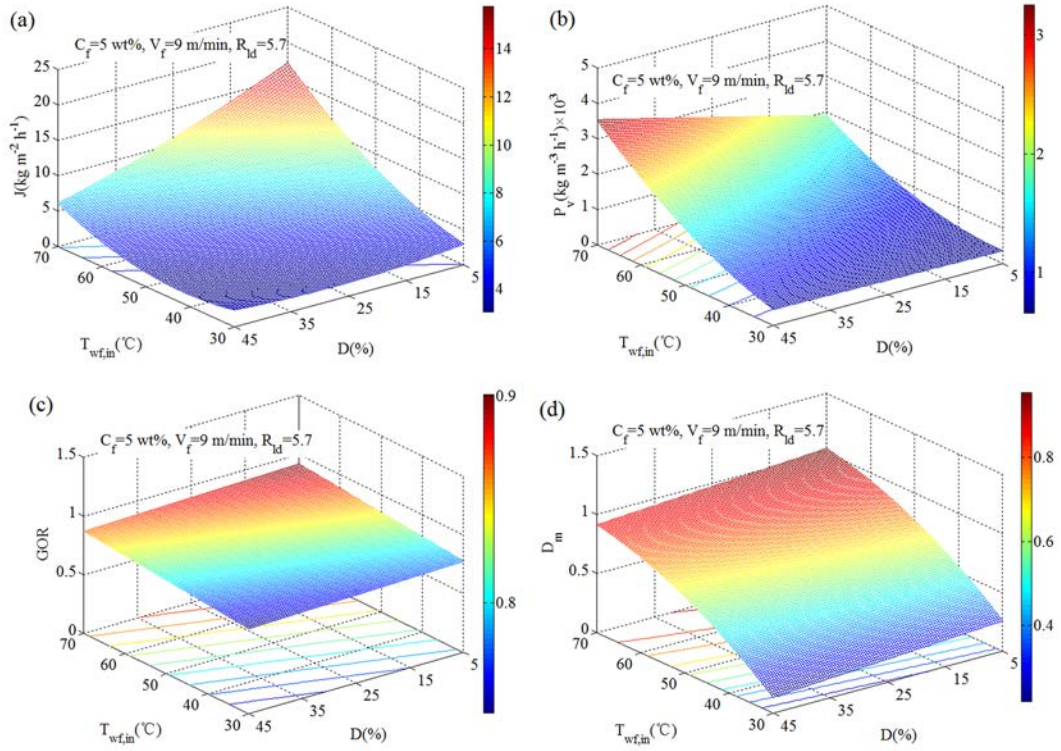

Fig. 6. Effects of feed inlet temperature ($T_{wf,in}$) and module packing density (D) on (a) permeate flux (J), (b) water productivity per unit volume of module (P_v), (c) gained output ratio (GOR), and (d) comprehensive index (D_m) in 3D response surface plots.

3.2.3. Binary effect of feed inlet temperature and length-diameter ratio of module

Fig. 7 (a-d) presents the response surface plot of permeate flux (J), water productivity per unit volume of module (P_v), gained output ratio (GOR), and comprehensive index (D_m) as a function of feed inlet temperature ($T_{wf,in}$) and length-diameter ratio of module (R_{ld}). As can be seen, there is an intensive interaction effect of $T_{wf,in}$ and R_{ld} on all the objectives.

In Fig. 7 (a), J rises to a much high value when $T_{wf,in}$ is high and R_{ld} is small. The decrease of R_{ld} from 8.5 to 2.9 at $T_{wf,in}$ of 70°C leads to 64.1% increase of J. This is attributed to a gradual temperature drop and thereof a water flux declines along membrane fiber length induced by water evaporation. Similarly, decreasing R_{ld} leads to the improvement of P_v. This is due to that the shorter membrane module, the higher average temperature on the feed side of membrane (Cheng et al., 2008). The improvement of P_v is more significant at high $T_{wf,in}$. For instance, when $T_{wf,in}$ is 40°C, decreasing R_{ld} from 8.5 to 2.9 leads to 44.1% increase in P_v. For the same range of R_{ld}, the P_v increases by 140% at a $T_{wf,in}$ of 70°C. The improvement of P_v by increasing $T_{wf,in}$ is also more

significant at lower values of R_{ld}. This means that the combination of high $T_{wf,in}$ and low R_{ld} is needed to achieve a significant improvement of J and P_v.

As shown in Fig. 7 (c), the decrease of R_{ld} leads to an increase of *GOR* and the positive function becomes stronger at higher $T_{wf,in}$. For instance, the decrease of R_{ld} from 8.5 to 2.9 at 70°C of $T_{wf,in}$ leads to 53.7% increase of *GOR*. With the same variation of R_{ld}, *GOR* only increases by 13.8% at 40°C of $T_{wf,in}$. Zhang et al. (Zhang et al., 2016) also found that the thermal efficiency in VMD process at 70°C of $T_{wf,in}$ decreased by increasing module length. It was believed that increasing module length would lead to the decrease of outlet temperature of membrane module. This causes the enlarged difference between feed inlet temperature ($T_{wf,in}$) and outlet temperature ($T_{wf,out}$) along membrane module. As a result, the average temperature on the feed side of membrane decreases, which leads to a decrease of average mass transport driving force. Thereof, water productivity decreases which causes a decline of the *GOR*. In Fig. 7 (c), it can also be observed that the effect of $T_{wf,in}$ on *GOR* is weak when R_{ld} is large. This means that only when R_{ld} is small, the increase of $T_{wf,in}$ is efficient in improving *GOR*.

Fig. 7 (d) shows that the increment in D_m with decreasing R_{ld} at higher $T_{wf,in}$ is greater than that at lower $T_{wf,in}$ values. The trend results from the more dramatic increase of all J, P_v, and *GOR* by decreasing R_{ld} at higher level of $T_{wf,in}$. Therefore, the combination of a high feed temperature with a short module is a great strategy for achieving high values of D_m which substantially means a high comprehensive performance of VMD.

In brief, the interaction effect of $T_{wf,in}$ and R_{ld} are key important factors influencing all the objectives. High $T_{wf,in}$ and small R_{ld} could lead to distinct improvement of comprehensive performance of MD no matter on water permeate flux through membrane, water productivity of module, and thermal efficiency of the desalination process.

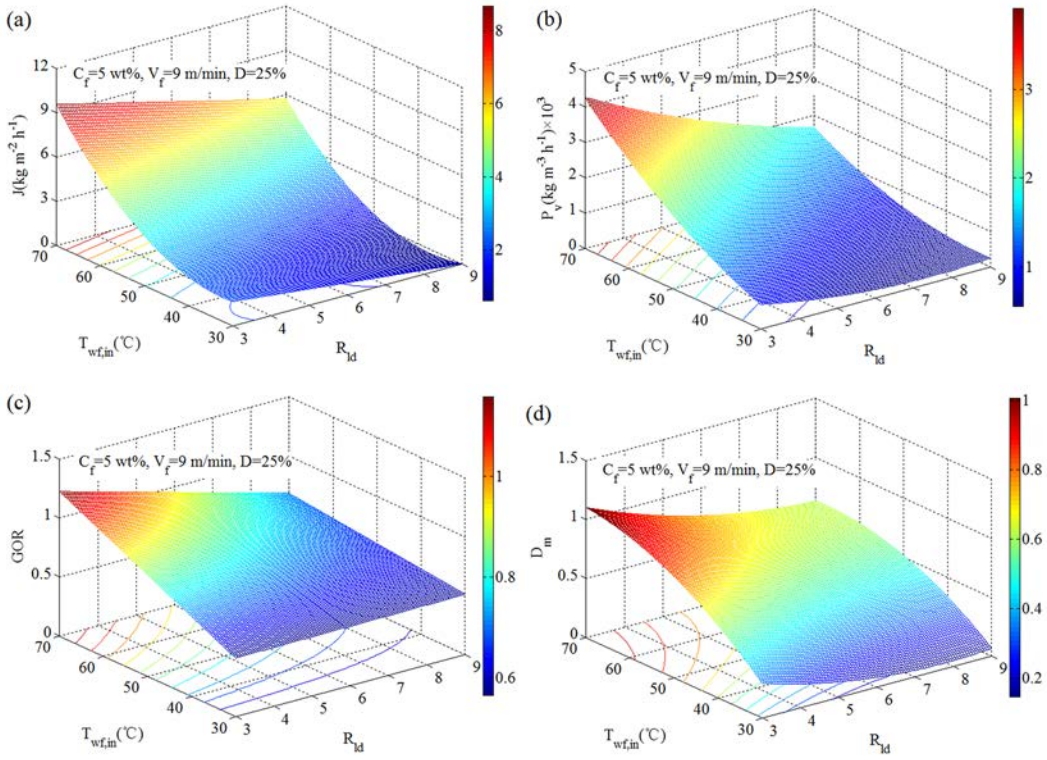

Fig. 7. Effects of feed inlet temperature ($T_{wf,in}$) and length-diameter ratio of module (R_{ld}) on (a) permeate flux (J), (b) water productivity per unit volume of module (P_v), (c) gained output ratio (GOR), and (d) comprehensive index (D_m) in 3D response surface plots.

3.2.4. Binary effect of feed inlet temperature and feed concentration

Fig. 8 shows the interaction effect of feed inlet temperature ($T_{wf,in}$) and feed concentration (C_f) on permeate flux (J), water productivity per unit volume of module (P_v), gained output ratio (GOR), and comprehensive index (D_m). As can be seen, $T_{wf,in}$ and C_f have significant interaction effect on J and somewhat interaction effect on P_v, GOR, and D_m.

Fig. 8 (a) shows that J increases with the increase of $T_{wf,in}$ and the decrease of C_f. The increase of J with decreasing C_f is attributed to the increase of water activity in the feed aqueous solution resulting in a reduction of the vapor pressure (Equation (12)). At low $T_{wf,in}$, the effect of C_f on J is unremarkable. Wirth and Cabassud (Wirth and Cabassud, 2002) also found that the influence of salt concentration on the water flux in VMD process at low temperature was insignificant. Since J in VMD is not very sensitive to feed salt concentration at moderate $T_{wf,in}$, VMD is a feasible process to treat with high feed concentration solutions in this case. No matter at low or high C_f values, increasing $T_{wf,in}$ leads to an exponential increase of J. For instance,

increasing $T_{wf,in}$ from 30 to 70°C leads to 614% increase of J for C_f of 1 wt% and 253% increase for C_f of 9 wt%.

The increase of $T_{wf,in}$ also leads to exponential increase of P_v, as shown in Fig. 8 (b). The decrease of P_v with increasing C_f is gentle, which is assistant to the linear relation of J with water activity shown in Equation (12). In Fig. 8 (c), it can be observed that *GOR* increases linearly with the increase of $T_{wf,in}$ and the decrease of C_f. The decrease of *GOR* with C_f is related to boiling point elevation of the feed stream with increasing C_f and less pure water is produced (Chung et al., 2016).

Fig. 8 (d) shows that D_m increases with increasing $T_{wf,in}$ and decreasing C_f, which is consistent with the variation of J, P_v, and *GOR*. However, even at 9 wt% of high salt concentration, D_m is still attractively high due to the relative stable *GOR* and the positive effect of high $T_{wf,in}$. It means that VMD could feasibly treat with high salt concentration feed by combination with suitable operating temperature.

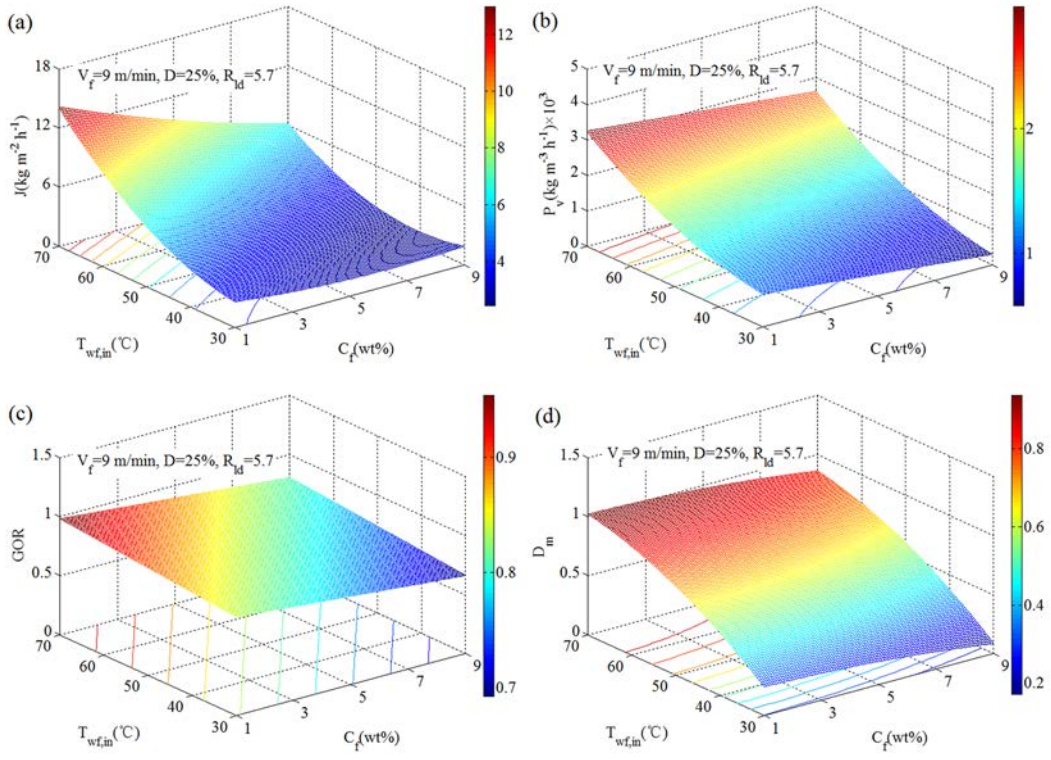

Fig. 8. Effects of feed inlet temperature ($T_{wf,in}$) and feed concentration (C_f) on (a) permeate flux (J), (b) water productivity per unit volume of module (P_v), (c) gained output ratio (*GOR*), and (d) comprehensive index (D_m) in 3D response surface plots.

3.2.5. Binary effect of feed concentration and feed velocity

The combined effect of feed concentration (C_f) and feed velocity (V_f) on permeate flux (J), water productivity per unit volume of module (P_v), gained output ratio (GOR), and comprehensive index (D_m) is presented in Fig. 9 (a-d). The binary factors show obvious interaction effect on J, P_v, and GOR.

Fig. 9 (a) shows that J increases by increasing V_f and decreasing C_f. The decrease of J with C_f is attributed to the decrease of water activity which reduces vapor pressure of the feed solution (Martinez, 2004; Martínez and Rodríguez-Maroto, 2007). High V_f will boost the flux especially when the C_f is high, because the concentration polarization could be reduced at high velocity (Yun et al., 2006). For instance, the increase of V_f from 1 to 17 m/min causes an increase of J to 1.6-fold when C_f is 1wt%, and increases to 2.5-fold when C_f rises to 9 wt%. This is due to the slight exponential increase of membrane flux with decreasing feed concentration at feed/membrane interface (Lei et al., 2005). Moreover, the reduction of J with the increase of C_f becomes gradually slight when increasing V_f. The permeate flux decreases by 24.1% when C_f increases from 5 to 9 wt% at V_f of 1 m/min. For the same range of C_f, the permeate flux reduces only by 9.4% at V_f of 17 m/min. This means that increasing V_f is an efficient way to keep relatively high permeate flux when treating with high concentration solution.

As shown in Fig. 9 (b), P_v decreases almost linearly with increasing C_f, which is consistent with the observations in Fig. 8 (b). Figs. 9 (c) and (d) show that the effect of C_f and V_f on GOR and D_m is insignificant. GOR and D_m increase slightly with the decrease in C_f and V_f.

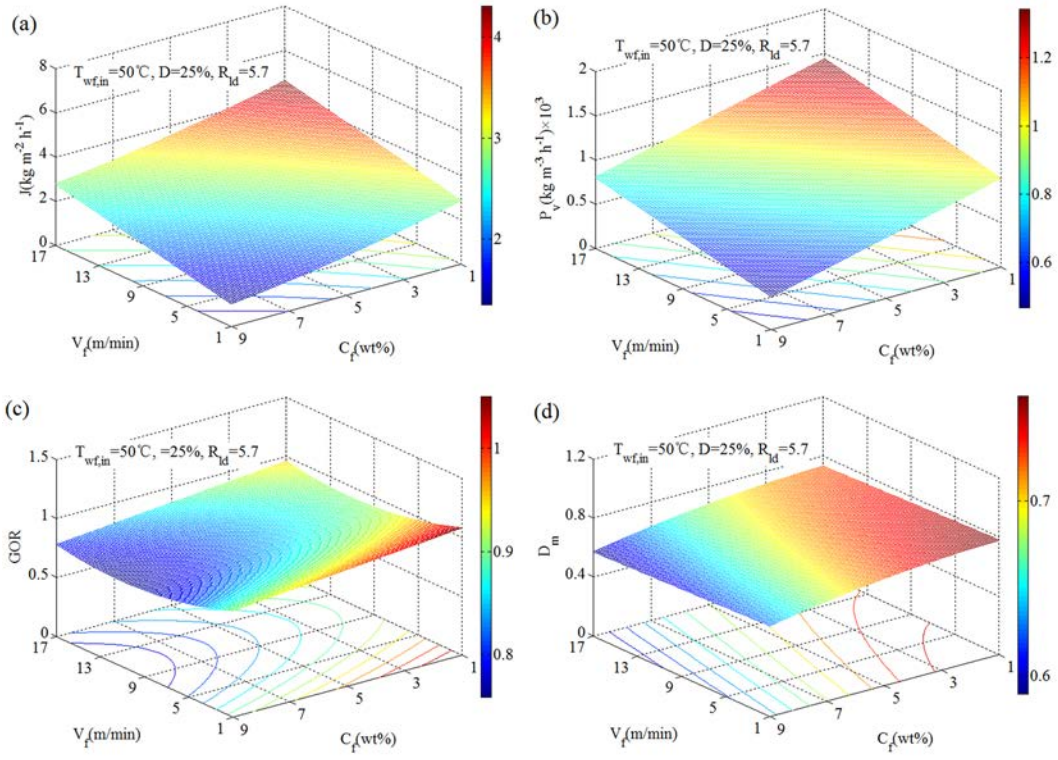

Fig. 9. Effects of feed concentration (C_f) and feed velocity (V_f) on (a) permeate flux (J), (b) water productivity per unit volume of module (P_v), (c) gained output ratio (GOR), and (d) comprehensive index (D_m) in 3D response surface plots.

3.3. Single- and multi-objective optimization of VMD process

Within the investigated region of the variables shown in Table 2, the optimum conditions determined with Matlab function are presented in Table 11. The GA-Genetic Algorithm in Matlab function module is used to solve the maximum value and optimum condition through finite iterations. In the single-objective optimization procedure, the optimum value of $T_{wf,in}$ is at its highest value in the designated range and the other four variables are either at their highest value or their lowest value in their designated range.

The verification experiments were conducted to confirm the validity of optimization procedure. The comparison between the experimental and predicted values of J, P_v, and GOR are shown in Table 11. It can be seen that the predicted results of J, P_v, and GOR based on simplified RS-models are in well agreement with the experimental results. The derivations were only 2.8% and 4.7% for J and P_v, respectively. The experimental value of GOR is 0.98 under optimum conditions, in comparison of the GOR values of VMD process varied from 0.80 to 0.93 (Hassan et

al., 2016; Summers et al., 2012). It means that under the optimum conditions, the thermal efficiency is high and the energy loss in the membrane module can be neglected.

Table 11. Single-objective optimum parameters and the corresponding average values of permeate flux (J), water productivity per unit volume of module (P_v), and gained output ratio (GOR).

Objective	$T_{wf,in}$, °C	C_f, wt%	V_f, m/min	D, %	R_{ld}	Experimental	Predicted
J, kg/(m^2•h)	70	1	17	5	2.9	24.2	23.5
P_v, kg/(m^3•h)	70	1	17	45	2.9	6187	5893
GOR	70	1	1	5	2.9	0.98	1.35

Furthermore, the maximum value of D_m was also determined to be 1.26 using Matlab function in a multi-objective optimization procedure. Under the optimum conditions for D_m, the new results of J, P_v, and GOR from experiment and prediction are displayed in Table 12. The experimental results and predicted responses also agree well. The derivations were only 9.6%, 5.4%, and 5.2% for J, P_v, and GOR, respectively. By comparing Table 11 to Table 12, it can be seen that the experimental values of the objectives under multi-objective optimum conditions were lower than those under single-objective optimum conditions. It means that the changes in the level of an influencing factor may improve one response but have a negative effect on another.

Table 12. Multi-objective optimum parameters and the corresponding average values of permeate flux (J), water productivity per unit volume of module (P_v), and gained output ratio (GOR).

$T_{wf,in}$,	C_f,	V_f,	D,	R_{ld}	J, kg/(m^2•h)		P_v, kg/(m^3•h)		GOR	
°C	wt%	m/min	%		$J_{exper.}$	$J_{pred.}$	$P_{vexper.}$	$P_{vpred.}$	$GOR_{exper.}$	$GOR_{pred.}$
70	1	17	20	2.9	15.0	16.6	4853	4590	0.91	0.96

In Table 13, the influence of the different combinations of the weight coefficients (in Table 6) on the optimum results is present. The maximum D_m values and the corresponding operation parameters calculated from the regression equations are 1.29 with NO. 3 combinations ($T_{wf,in}$ of 70°C, C_f of 1 wt%, V_f of 17 m/min, D of 5.2%, and R_{ld} of 2.9) and NO. 10 combinations ($T_{wf,in}$ of 70°C, C_f of 1 wt%, V_f of 17 m/min, D of 12.6%, and R_{ld} of 2.9). It is interesting that at the different weight coefficient combinations, if the D_m achieves the maximum value, the $T_{wf,in}$, C_f, V_f, and R_{ld} are the same values, but D varies. It is due to that the greater values of $T_{wf,in}$ and V_f and lower values of C_f and R_{ld} are favorable for the J, P_v, and GOR, as shown in Figs. 5, 7, 8, and 9.

However, as shown in Fig. 6, the D shows negligible effect on the GOR, but shows great influence on the trade-off between J and P_v. Therefore, with the given weight coefficients, it needs to optimize the packing density, D to achieve the maximum D_m.

Table 13. Multi-objective optimum parameters and the results corresponding to the different weight coefficients shown in Table 6.

NO.	$T_{wf,in}$, °C	C_f, wt%	V_f, m/min	D, %	R_{ld}	J, kg/(m^2•h)	P_v, kg/(m^3•h)	GOR	$D_{m,max}$
1	70	1	17	20	2.9	16.6	4589.7	0.97	1.26
2	70	1	17	19.3	2.9	16.8	4168.7	0.97	1.01
3	70	1	17	5.2	2.9	23.4	3222.7	0.98	1.29
4	70	1	17	15	2.9	18.6	3880.2	0.96	1.21
5	70	1	17	12.5	2.9	19.8	3712.5	0.96	1.25
6	70	1	17	13.5	2.9	19.3	3779.6	0.96	1.19
7	70	1	17	8.6	2.9	21.6	3450.8	0.97	1.05
8	70	1	17	5.9	2.9	23.0	3269.7	0.97	1.26
9	70	1	17	5	2.9	23.5	3209.3	0.96	1.07
10	70	1	17	12.6	2.9	19.7	3719.2	0.96	1.29

4. Conclusions

In this study, the average permeate flux (J), water productivity per unit volume of module (P_v), gained output ratio (GOR), and a comprehensive index (D_m) of VMD process were modeled and optimized as function of operating and module configuration parameters by response surface methodology. The multi-objective optimization was performed by introducing a comprehensive index (D_m) as a global desirability based on desirability function approach. The multiple regression models were simplified and statistically validated by analysis of variance. The predicted results based on the models provide insights into the effect of the interactions between the operating parameters and module configuration parameters on the objectives.

(1) The RS-models provided a simple method for predicting J, P_v, and GOR of VMD. Under optimum conditions predicted by single-objective optimization procedure, J is increased from the minimum value of <1 kg/(m^2•h) to 24 kg/(m^2•h), P_v from 209 to 6187 kg/(m^3•h), and GOR from

0.68 to 0.98 within the investigated range of the variables.

(2) Under the multi-response optimum conditions where the comprehensive index (D_m) reaches to a maximum value, J, P_v, and GOR values are 15.0 kg/(m^2•h), 4850 kg/(m^3•h) and 0.91, respectively. The lower values of J, P_v, and GOR compared to their maximum ones under specific single-objective optimum conditions is due to the "trade-off" phenomenon, that is, the changes in the level of an influencing factor may improve one response but have a negative effect on another.

(3) Among the investigated factors, feed inlet temperature ($T_{wf,in}$) and its interaction effect with module parameters play dominant roles on MD performance. The synergistic effect of high $T_{wf,in}$ with high feed velocity (V_f) are vital to improve J and P_v significantly. High GOR can be realized under the synergistic effect of increasing $T_{wf,in}$ and V_f and the improvement of GOR by increasing $T_{wf,in}$ is more efficient at smaller R_{ld}. Moreover, increasing $T_{wf,in}$ absolutely compensates the decrease of J and P_v resulting from increasing salt concentration of feed (C_f), and due to the mild effect of C_f on GOR, VMD presents attractive potential to treat with high salt concentration feed solution. Therefore, the combination of high $T_{wf,in}$ with high V_f and low R_{ld} basically meets a desired performance of VMD process on high level of water production and thermal efficiency.

(4) Increasing module packing density (D) plays a complicated role on VMD performance. Increasing D leads to increase of P_v with negligible impact on GOR. Although J may be reduced by increasing D, the improvement of P_v is achieved which is more attractive in practical application of VMD. Moreover, to increase V_f and removing speed of permeate vapor out of module is an efficient way to alleviate concentration and temperature polarization of MD process for the improvement of J. This will increase P_v effectively even at relatively high D. Therefore, the combination of high $T_{wf,in}$, V_f, and D and low R_{ld} is essential to achieve comprehensively high performance of MD process, which could be followed to scale up MD process in its desalination application.

1

Nomenclature

T	temperature, °C	N	test points
C	concentration, wt%	M_c	rotation design points
V	flow velocity, m/min	M_r	star points
D	module packing density, %	M_0	center points
R_{ld}	length-diameter ratio of module		
ΔW	mass variation, kg/h		
A	surface area of membrane, m^2	*Subscripts*	
t	time, h	f	feed
l	effective length of membrane module, m	d	distillate
$d_{i,m}$	inner diameter of membrane module, m	*max*	maximum
J	average permeate flux, kg/(m^2•h)	*min*	minimum
P_v	water productivity per unit volume of module, kg/(m^3•h)		
D_m	comprehensive index	*Abbreviations*	
m	mass flow rate, kg/h	*RSM*	response surface methodology
R^2	fitting coefficient	*GOR*	gained output ratio
t	time, h	*ARE*	average relative error
$C_{p,f}$	specific heat capacity, kJ/(kg•°C)	*MPSD*	Marquradt's percent standard deviation
z	actual parameter value	*ANOVA*	analysis of variance
d_i	normalized variable	*DF*	degree of freedom
g	weight coefficient		

2

Acknowledgements

This work was supported by the National Natural Science Foundation of China [grant numbers 21676210]. Authors would also like to thank Prof. Xiaolong Lv and Prof. Chunrui Wu from Tianjin Polytechnic University for providing PVDF hollow fiber membrane modules.

References

Abu-Zeid, M.A.E.R., Zhang, Y., Dong, H., Zhang, L., Chen, H.L., Hou, L., 2015. A comprehensive review of vacuum membrane distillation technique. Desalination 356, 1–14.

Alkhudhiri, A., Darwish, N., Hilal, N., 2012. Membrane distillation: A comprehensive review. Desalination 287, 2–18.

Bezerra, M.A., Santelli, R.E., Oliveira, E.P., Villar, L.S., Escaleira, L.A., 2008. Response surface methodology (RSM) as a tool for optimization in analytical chemistry. Talanta 76, 965–977.

Boubakri, A., Hafiane, A., Bouguecha, S.A.T., 2014. Application of response surface methodology for modeling and optimization of membrane distillation desalination process. J. Ind. Eng. Chem. 20, 3163–3169.

Bouchrit, R., Boubakri, A., Hafiane, A., Bouguecha, S.A.T., 2015. Direct contact membrane distillation: Capability to treat hyper-saline solution. Desalination 376, 117–129.

Cao, W., Liu, Q., Wang, Y., Mujtaba, I.M., 2016. Modeling and simulation of VMD desalination process by ANN. Comput. Chem. Eng. 84, 96–103.

Cerneaux, S., Struzyńska, I., Kujawski, W.M., Persin, M., Larbot, A., 2009. Comparison of various membrane distillation methods for desalination using hydrophobic ceramic membranes. J. Memb. Sci. 337, 55–60.

Chang, H., Liau, J.S., Ho, C.D., Wang, W.H., 2009. Simulation of membrane distillation modules for desalination by developing user's model on Aspen Plus platform. Desalination 249, 380–387.

Chang, J., Zuo, J., Zhang, L. O'Brien, G.S., Chung, T.S., 2017. Using green solvent, triethyl phosphate (TEP), to fabricate highly porous PVDF hollow fiber membranes for membrane distillation. J. Memb. Sci. 539, 295–304.

Cheng, D., Gong, W., Li, N., 2016. Response surface modeling and optimization of direct contact membrane distillation for water desalination. Desalination 394, 108–122.

Cheng, L.H., Wu, P.C., Chen, J., 2008. Modeling and optimization of hollow fiber DCMD module for desalination. J. Memb. Sci. 318, 154–166.

Chung, H.W., Swaminathan, J., Warsinger, D.M., Lienhard V, J.H., 2016. Multistage vacuum membrane distillation (MSVMD) systems for high salinity applications. J. Memb. Sci. 497,

128–141.

Cojocaru, C., Khayet, M., 2011. Sweeping gas membrane distillation of sucrose aqueous solutions: Response surface modeling and optimization. Sep. Purif. Technol. 81, 12–24.

Cojocaru, C., Khayet, M., Zakrzewska-Trznadel, G., Jaworska, A., 2009. Modeling and multi-response optimization of pervaporation of organic aqueous solutions using desirability function approach. J. Hazard. Mater. 167, 52–63.

Costa, N.R., Lourenço, J., Pereira, Z.L., 2011. Desirability function approach: A review and performance evaluation in adverse conditions. Chemom. Intell. Lab. Syst. 107, 234–244.

Drioli, E., Ali, A., Macedonio, F., 2015. Membrane distillation: Recent developments and perspectives. Desalination 356, 56–84.

Eykens, L., Sitter, K.D., Dotremont, C., Pinoy, L., Bruggen, B.V.D., 2016. How to optimize the membrane properties for membrane distillation: a review. Ind. Eng. Chem. Res. 55, 9333−9343.

El-Bourawi, M.S., Ding, Z., Ma, R., Khayet, M., 2006. A framework for better understanding membrane distillation separation process. J. Memb. Sci. 285, 4–29.

Fan, H., Peng, Y., 2012. Application of PVDF membranes in desalination and comparison of the VMD and DCMD processes. Chem. Eng. Sci. 79, 94–102.

Guan, G., Yang, X., Wang, R., Field, R., Fane, A.G., 2014. Evaluation of hollow fiber-based direct contact and vacuum membrane distillation systems using aspen process simulation. J. Memb. Sci. 464, 127–139.

Hassan, M.I., Brimmo, A.T., Swaminathan, J., Lienhard V, J.H., Arafat, H.A., 2016. A new vacuum membrane distillation system using an aspirator: concept modeling and optimization. Desalin. Water Treat. 57, 12915–12928.

He, Q., Li, P., Geng, H., Zhang, C., Wang, J., Chang, H., 2014. Modeling and optimization of air gap membrane distillation system for desalination. Desalination 354, 68–75.

Hitsov, I., Maere, T., De Sitter, K., Dotremont, C., Nopens, I., 2015. Modelling approaches in membrane distillation: A critical review. Sep. Purif. Technol. 142, 48–64.

Khayet, M., 2011. Membranes and theoretical modeling of membrane distillation: A review. Adv. Colloid Interface Sci. 164, 56–88.

Khayet, M., Cojocaru, C., Baroudi, A., 2012. Modeling and optimization of sweeping gas

membrane distillation. Desalination 287, 159–166.

Khayet, M., Cojocaru, C., García-Payo, C., 2007. Application of Response Surface Methodology and Experimental Design in Direct Contact Membrane Distillation. Ind. Eng. Chem. Res. 46, 5673–5685.

Lawson, K.W., Lloyd, D.R., 1997. Membrane Distillation. J. Memb. Sci. 124, 1–25.

Lei, Z., Chen, B., Ding, Z., 2005. Special Distillation Processes, Published by Elsevier Science Technology, London.

Li, B., Sirkar, K.K., 2005. Novel membrane and device for vacuum membrane distillation-based desalination process. J. Memb. Sci. 257, 60–75.

Lian, B., Wang, Y., Le-Clech, P., Chen, V., Leslie, G., 2016. A numerical approach to module design for crossflow vacuum membrane distillation systems. J. Memb. Sci. 510, 489–496.

Lipnizki, F., Field, R.W., 2001. Mass transfer performance for hollow fibre modules with shell-side axial feed flow: using an engineering approach to develop a framework. J. Memb. Sci. 193, 195–208.

Martínez, L., 2004. Comparison of membrane distillation performance using different feeds. Desalination 168, 359–365.

Martínez, L., Rodríguez-Maroto, J.M., 2007. On transport resistances in direct contact membrane distillation. J. Memb. Sci. 295, 28–39.

Mohammadi, T., Kazemi, P., Peydayesh, M., 2015. Optimization of vacuum membrane distillation parameters for water desalination using Box–Behnken design. Desalin. Water Treat. 56, 2306–2315.

Mohammadi, T., Safavi, M.A., 2009. Application of Taguchi method in optimization of desalination by vacuum membrane distillation. Desalination 249, 83–89.

Pasandideh, S.H.R., Niaki, S.T.A., 2006. Multi-response simulation optimization using genetic algorithm within desirability function framework. Appl. Math. Comput. 175, 366–382.

Perry, R.H., Green, D.W., 1998. Perry’s chemical engineers’ handbook, McGraw-Hill International Editions, New York.

Qian, C., Zhang, M., Chen, Y., Wang, R., 2014. A quantitative judgement method for safety admittance of facilities in chemical industrial parks based on G1-variation coefficient method. Procedia Eng. 84, 223–232.

Ravikumar, K., Pakshirajan, K., Swaminathan, T., Balu, K., 2005. Optimization of batch process parameters using response surface methodology for dye removal by a novel adsorbent. Chem. Eng. J. 105, 131–138.

Shirazi, M.M.A., Kargari, A., Ismail, A.F., Matsuura, T., 2016. Computational Fluid Dynamic (CFD) opportunities applied to the membrane distillation process: State-of-the-art and perspectives. Desalination 377, 73–90.

Summers, E.K., Arafat, H.A., Lienhard V, J.H., 2012. Energy efficiency comparison of single-stage membrane distillation (MD) desalination cycles in different configurations. Desalination 290, 54–66.

Swaminathan, J., Chung, H.W., Warsinger, D.M., Lienhard V, J.H., 2016. Membrane distillation model based on heat exchanger theory and configuration comparison. Appl. Energy 184, 491–505.

Samantaray, P.K., Madrasb, G., Bose, S., 2018. PVDF/PBSA membranes with strongly coupled phosphonium derivatives and graphene oxide on the surface towards antibacterial and antifouling activities. J. Memb. Sci. 548, 203–214.

Tang, Y., Li, N., Liu, A., Ding, S., Yi, C., Liu, H., 2012. Effect of spinning conditions on the structure and performance of hydrophobic PVDF hollow fiber membranes for membrane distillation. Desalination 287, 326–339.

Tricco, A.C., Zarin, W., Antony, J., Hutton, B., Moher, D., Sherifali, D., Straus, S.E., 2016. An international survey and modified Delphi approach revealed numerous rapid review methods. J. Clin. Epidemiol. 70, 61–67.

Wang, P., Chung, T.S., 2015. Recent advances in membrane distillation processes: Membrane development, configuration design and application exploring. J. Memb. Sci. 474, 39–56.

Wirth, D., Cabassud, C., 2002. Water desalination using membrane distillation : comparison between inside/out and outside/in permeation. Desalination 147, 139–145.

Y. Shin, J. Choi, T. Lee, J. Sohn, S.L., 2016. Optimization of dewetting conditions for hollow fiber membranes in vacuum membrane distillation. Desalin. Water Treat. 57,7582–7592.

Yang, X., Wang, R., Shi, L., Fane, A.G., Debowski, M., 2011. Performance improvement of PVDF hollow fiber-based membrane distillation process. J. Memb. Sci. 369, 437–447.

Yun, Y., Ma, R., Zhang, W., Fane, A.G., Li, J., 2006. Direct contact membrane distillation

mechanism for high concentration NaCl solutions. Desalination 188, 251–262.

Zhang, Y., Peng, Y., Ji, S., Li, Z., Chen, P., 2015. Review of thermal efficiency and heat recycling in membrane distillation processes. Desalination 367, 223–239.

Zhang, Y., Peng, Y., Ji, S., Wang, S., 2016. Numerical simulation of 3D hollow-fiber vacuum membrane distillation by computational fluid dynamics. Chem. Eng. Sci. 152, 172–185.